WPJET2-PR(17) 18992

S Fazinic et al.

Ion micro-beam analyses of dust particles and co-deposits from JET with ITER-like wall

Preprint of Paper to be submitted for publication in Analytical Chemistry

This work has been carried out within the framework of the EUROfusion Consortium and has received funding from the Euratom research and training programme 2014-2018 under grant agreement No 633053. The views and opinions expressed herein do not necessarily reflect those of the European Commission.

Ion micro-beam analyses of dust particles and co-deposits from JET with ITER-like wall

Stjepko Fazinić*[1], Tonči Tadić[1], Marin Vukšić[1], Marek Rubel[2], Per Petersson[2], Elżbieta Fortuna-Zaleśna[3], Anna Widdowson[4] and JET Contributors[5]

[1]Ruđer Bošković Institute, Bijenička 54, 10000 Zagreb, Croatia.

[2]Royal Institute of Technology (KTH), Department of Fusion Plasma Physics, School of Electrical Engineering, Teknikringen 31, 100 44 Stockholm, Sweden.

[3]Warsaw University of Technology, Faculty of Materials Science and Technology, Woloska 141, 02-507 Warsaw, Poland.

[4]Culham Centre for Fusion Energy, Culham Science Centre, Abingdon, OX14 3DB, UK.

[5]See the author list of "X. Litaudon et al 2017 Nucl. Fusion 57 102001".

E-mail: stjepko.fazinic@irb.hr

Phone: +385 99 3174866

ABSTRACT: Generation of metal dust in the JET tokamak with the ITER-like wall and morphology of particles is a topic of vital interest to next-step fusion devices because of safety issues in plasma operation. Simultaneous Nuclear Reaction Analysis (NRA) and Particle-Induced X-ray Emission (PIXE) with focused 4 MeV ^{3}He micro-beam were used together with electron microscopy methods to analyse dust collected from the deposition zone on the inner divertor tile. The particles found are composed of a mix of co-deposited species up to 100 x 120 μm in size with the thickness of 30-40 μm. The main constituents are: deuterium from the fusion fuel, beryllium and tungsten originating from the main plasma-facing components, nickel and chromium from Inconel grills of antennas for auxiliary plasma heating. Elemental concentrations of major and minor elements have been estimated by semi-quantitative iterative NRA-PIXE analysis. NRA-PIXE data acquisition and analytical procedures are presented and main results elaborated.

INTRODUCTION

Plasma-surface interaction processes in devices for controlled thermonuclear fusion cause erosion of plasma-facing components (PFC). This is followed by migration and re-deposition of eroded species and, as a consequence, the modification of wall materials and fusion plasma. Plasma dynamics in a tokamak includes transport of eroded particles down toward the divertor. Joint European Torus (JET) is the world's largest operating tokamak with the closest proximity (shape of the vessel and divertor) to the International Thermonuclear Experimental Reactor (ITER), which is under construction in France. JET has unique capabilities to handle beryllium and radioactive tritium. Wall materials are beryllium (Be) in the main chamber wall and tungsten (W) in the divertor[1,2]. The same material configuration will be in ITER[3,4], therefore JET with its ITER-like wall (JET-ILW) serves as a large-scale test bed for plasma operation with metal walls.

A certain part of material eroded from the walls will be converted into dust. Its formation in present-day machines does not pose operation issues, because quantities are small, especially in the presence of metal walls. In JET it is around 1 g per experimental campaign comprising 19 – 25 h[5,6]. However, in ITER generation of large quantities of loose particles will create serious problems, because dust is a radiological (T and activation products) and toxic (e.g. Be) hazard. Typical dust particle size is likely to be < 150 μm. It is chemically reactive with water and oxygen in the case of water leak or massive air ingress. For that reason comprehensive characterization of wall components and dust has been carried out in current fusion devices. A list of papers published until year 2011 mostly for carbon wall machines has been compiled by B. Braams[3], while recent works deal with JET-ILW[6,7] and ASDEX Upgrade[8].

The goal of this work is to perform micro-analysis of dust from JET by means of ion-beam analytical methods and with the aid of SEM methods. Ion micro-beam has been used in the past for studies of PFC surfaces[9-13], but to our knowledge this is the first work where these techniques have been applied for characterisation of locally sampled dust from fusion devices. Therefore, methodology of studies will be introduced, following by the presentation of semi-quantitative concentrations obtained for major and trace elements in the analysed material.

EXPERIMENTAL SECTION

Dust was sampled using a sticky carbon pad from the inner divertor tile after the second ILW campaign (2013-2014) comprising 19.5 h of plasma operation (13.5 h of X-point plasma) with total energy input of 201 GJ. A drawing in Figure 1 (a) shows the poloidal divertor cross-section with marked positions of dust sampling. In the insert one perceives a plastic cup at which bottom there is a tab equipped with a sticky pad. This procedure delivers samples ready for further analyses by ion or electron beams. An image in Figure 1 (b) presents the High Field Gap Closure tile (HFGC, Tile 0) from the inner divertor. The tile has two distinct areas: a part without deposition on the shiny tungsten coating and a zone covered by co-deposit containing a mixture of elements. Sampling, marked with a red spot, was done in that deposition zone. In the insert there is an actual sample with a marked area of micro-analysis. One may perceive only small amount of matter sticking to the pad (especially shiny region at the left), thus indicating that dust and/or co-deposit was sticking well to the tile surface.

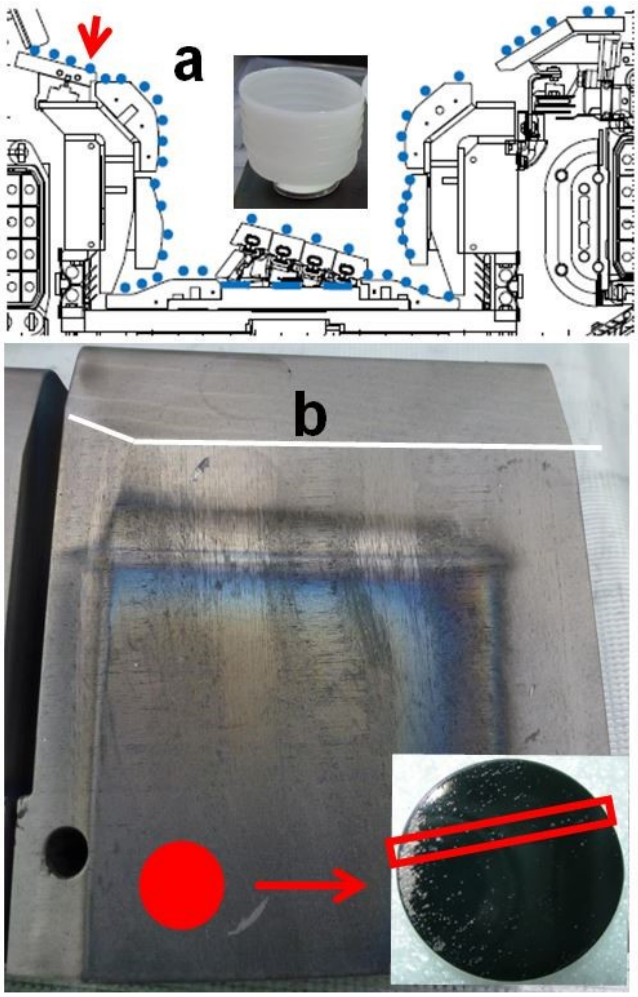

Figure 1 (a) Poloidal cross-section of the JET-ILW divertor with marked position of dust sampling; (b) inner divertor tile and the position of dust sampling for studies presented in the paper. The insert shows the carbon sticky pad used for dust sampling.

It was expected that the sample could contain D, Be, W, Cr, Fe, Ni, and possibly some Mo, Cu, N, C and/or O, in line with the surface analysis of tiles and wall probes exposed during the first JET ILW campaign[14-16]. Therefore, those have provided bases for the selection of dust analysis conditions with micro-beams.

Dust morphology studies were performed at the Warsaw University of Technology, Poland. For this purpose scanning electron microscopy (SEM, Hitachi SU-8000 FE-SEM) combined with energy-dispersive X-ray spectroscopy using silicon drift detector (EDS, Thermo Scientific Ultra Dry) capable of detecting both beryllium and heavier elements was used. The electron beam energy in the studies was typically 10 keV, but on several occasions low energy (1 or 2 keV) was applied. SEM EDS can provide only surface information in the depth of up to 1 μm and cannot detect deuterium presence in the samples.

Therefore we decided to use Ion Beam Analysis (IBA) methods to detect all the above elements expected in the samples, including deuterium. In addition, compared to SEM, IBA methods can provide information on the presence of these elements in larger depths comparable with the expected dust particles' thickness. Among the IBA methods, Nuclear Reaction Analysis (NRA) can be used to detect light elements like deuterium, beryllium, carbon, etc. We selected to work with ^{3}He ion beam since the nuclear reaction D(^{3}He, ^{4}He)p is widely used to detect deuterium[17]. At the same time it can also be used for the detection of Be, C[18] and some other light elements like N and B. Simultaneously Particle Induced X-Ray Emission (PIXE) spectra can be measured to detect heavier elements. A 4 MeV ^{3}He ion beam was used since this is optimal energy for transmission through our accelerator system. At this energy reasonable NRA and PIXE yields can be achieved simultaneously with well-focused ions inside our ion microprobe.

IBA measurements were performed at the Ruđer Bošković Institute using ion microprobe facility[19]. However, standard ion microprobe chamber configuration was modified to allow simultaneous PIXE and NRA measurements with installed non-standard large area and large depth particle detector. ^{3}He ion beam from the Alphatross ion source was accelerated to 4 MeV by the 6 MV tandem electrostatic accelerator, and focused by a triplet magnetic quadrupole lens system to about 6 μm spot size and raster scanned over selected samples. The ^{3}He ion beam current was in the range between 50 and 100 pA. Ni and Cu grids (mesh 500 and 1000) were used to estimate the ion microbeam resolution and the size of the raster scan areas from two-dimensional (2D) distribution of Ni K and Cu L PIXE X-ray line intensities. Focused ^{3}He ion beam was scanned over a rectangular scan patterns with a size of 320x320 μm^2 and 128x128 pixels. Simultaneously NRA and PIXE spectra were collected.

PIXE spectra were collected using a 30 mm^2 Si(Li) detector with a 12.5 μm Be window placed at 135° relative to the beam direction at a distance of about 4 cm from the target and detector solid angle of 0.0176 sr. The effective detector X-ray energy resolution was about 160 eV (for the Mn Kα line). NRA spectra were detected by the Partially Depleted Silicon Surface Barrier detector (PDSSB) ORTEC BA-022-300-2000 with depletion depth of 2000 μm, with nominal active area of 300 mm^2 collimated to 230 mm^2 and placed at135 ±19 deg. The detector was positioned as close as possible to the sample to increase the solid angle for particle detection. The solid angle was determined by measuring simultaneously PIXE and RBS (Rutherford Back-Scattering) spectra of pure Ti and Ni thick foils and thin Cr film (48.5 μm/cm^2) on polyester backing using a focused 4 MeV ^{3}He ion beam in the same detector-sample geometry as for the actual measurements on the dust samples. The resulting detector solid angle was determined to be 0.462 sr. For NRA measurements in front of the PDSSB detector 9 μm thick titanium and 12 μm thick mylar foils were placed to absorb the low-energy elastically backscattered primary particles from the target and to reduce pile-up background. The whole setup was kept in the ion micro-beam chamber under vacuum (10^{-7} bar) produced by the turbo-molecular vacuum pump system.

PIXE and NRA data were digitally recorded with the SPECTOR data acquisition software[20] in a list file. Such list files were used for off-line analysis to create PIXE and NRA spectra from selected regions within the measured raster areas. Afterwards, NRA and PIXE spectra were analysed by the SIMNRA[21,22] and GUPIXWin software[23,24] packages. The large PDSSB detector aperture and solid angle resulted in a spread of exit and reaction angles. Therefore, NRA spectra simulations with SIMNRA were performed for scattering angles between 154 and 116 deg (i.e. for 135 ±19 deg). Final simulated spectra were obtained by the integration (summation) of such simulated spectra with respective weighting factors to account for geometrical effects due to this large detector solid angle.

Measured NRA spectra were simulated with the SIMNRA using differential cross-sections available from IBANDL database of the IAEA[25]. This database provides useful cross-sections for IBA methods, including NRA. However, differential cross-section data for reactions are available only for limited scattering angles. For example differential cross sections for D(^{3}He, ^{4}He)p reaction are available for 135 deg[26] and 86 deg[17]. Data for 135 deg are available for ^{9}Be(^{3}He, p$_0$)^{11}B only for ^{3}He energies of up to 2.49 MeV[27]. For larger ^{3}He energies data are available for 150 and 90 deg[28]. According to available data the difference of differential cross sections for this reaction for angles between 90 and 150 deg is small for the energies between 3 to 4 MeV, with the value of about 1 mb/sr[28]. In our measurement setup with the foils in front of the NRA detector, the peaks from thick targets coming from ^{9}Be(^{3}He, p$_0$)^{11}B and ^{9}Be(^{3}He,α$_0$)^{8}Be reactions are overlapped. Data for the later reaction are available for 90, 125 and 150 deg. Differential cross section value at 4 MeV is about 0.4 mb/sr at 125 deg and 0.6 mb/sr at 150 deg[29]. Data for ^{9}Be(^{3}He, p$_i$)11B (i=2-7) are available only for 90 deg[30]. Data for 9Be(^{3}He, α$_1$)^{8}Be are available only for the energies below 3.18 MeV. Therefore for semi-quantitative analysis of Be by SIMNRA we used only reactions ^{9}Be(^{3}He, p$_o$)^{11}B and ^{9}Be(^{3}He, α$_o$)^{8}Be, represented by the highest energy peak in the Be spectrum shown at the Figure 2. This Figure shows measured NRA

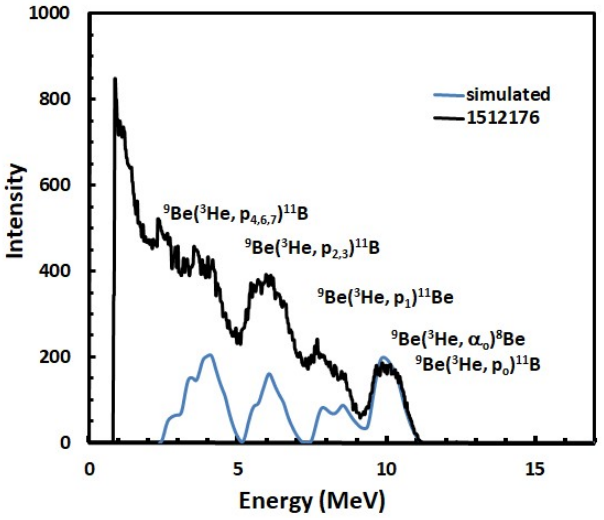

Figure 2 Measured NRA spectrum of 25 μm thick Be foil and simulated NRA spectrum obtained by SIMNRA with the correction due to large solid angle.

spectrum from 25 μm thick Be foil used as a standard. The simulation performed shows that the Be NRA signal is coming from the surface to the depth of about 1.8x10^{20} at/cm^2, which

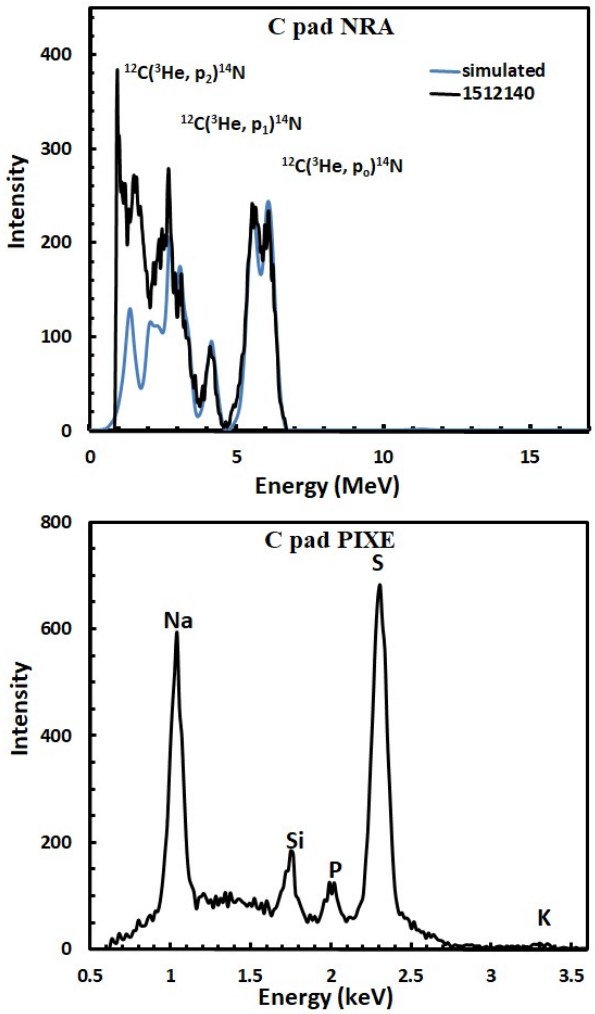

Figure 3 Measured NRA and PIXE spectra from the pad tape.

corresponds to the depth of 15 μm in Be (mass density 1.803 g/cm^3).

For nitrogen analysis, data are available on differential cross sections for ^{14}N(^{3}He, p$_i$)^{16}O (i=0-4) reactions and scattering angle of 135 deg[31] and for ^{14}N(^{3}He, α$_0$)^{13}N reaction also for 135 deg[32]. For carbon analysis, data are available on differential cross sections for ^{12}C(^{3}He, p$_i$)^{14}N (i=0-2) reactions and scattering angles of 90 and 159.4 deg[33,34], for ^{12}C(^{3}He,^{4}He)^{11}C reaction at 159.4 deg[33], and for ^{13}C(^{3}He, p^i)^{15}N (i=0-3) reactions and scattering angle of 150 deg[35]. Figure 3 shows NRA and PIXE spectra of carbon pad tape. NRA shows measured carbon spectrum from the pad together with simulated NRA spectrum obtained by SIMNRA with the geometrical correction due to large solid angle. Simultaneously collected PIXE spectrum shows clear presence of Na and S, with some Si, P and K contributions.

RESULTS AND DISCUSSION

A number of 2D scans was performed within the marked area shown in the insert of Figure 1(b), starting from the left side where majority of collected dust particles are located. Figure 4 shows 2D distribution maps of major elements from one of a number of selected scanned areas in this region with high density of dust particles. Figure 5 shows related simultaneously obtained PIXE and NRA spectra used to create those 2D elemental maps. Large number of dust particles of different sizes varying between several μm to about 60 μm is clearly seen. Beryllium and deuterium 2D maps are extracted from the NRA spectrum, which clearly shows also the presence of carbon. Majority of carbon signal originates from the sticky pad as well as Na, S, Si and K peaks in the corresponding PIXE spectrum which also shows that chromium, nickel, iron and tungsten are major elements present in these dust particles, together with some copper and titanium.

Off line analysis was performed by selecting the region of interest (ROI) corresponding to the pixels with the presence of tungsten in related W 2D map in Figure 4. Related PIXE and NRA spectra are shown at the Figure 5 in red and marked as 137r1. It is clearly seen that Be and D from NRA are correlated with W, Cr, Ni and Cu from PIXE while all these elements

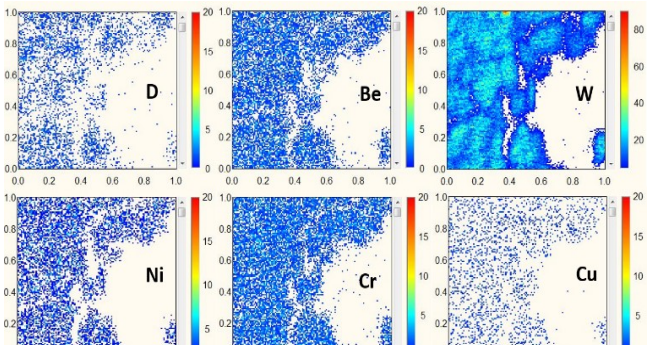

Figure 4 2D distribution maps of major elements from selected scanned area at the left side of the pad shown at Figure 1 in the region with high density of dust particles. Scan size is 320x320 μm^2 and resolution is 128x128 pixels.

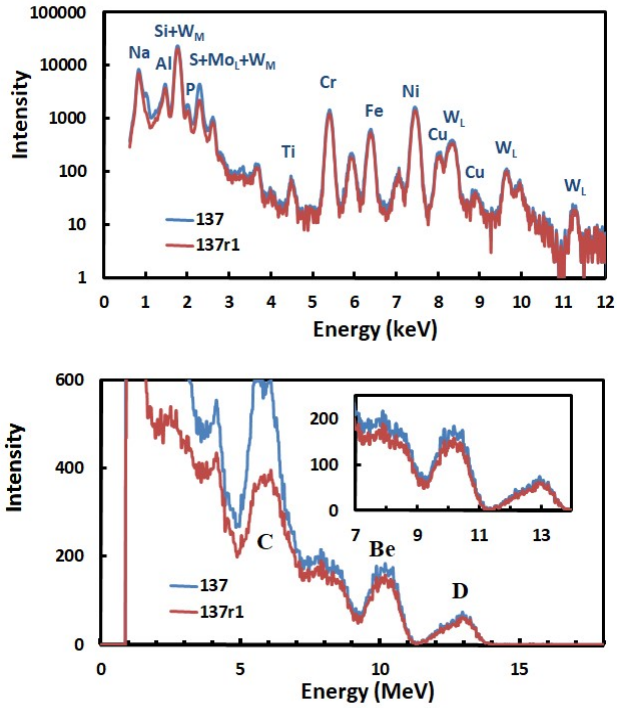

Figure 5 Respective PIXE and NRA spectra from the scanned area from Figure 4.

are correlated with dust particles. The peak at around channel 300 corresponding to carbon is considerably reduced within the selected ROI.

Elemental concentrations in dust particles were estimated from related NRA and PIXE spectra. For this purpose iterative procedure has been used after the calibration performed in a way as described earlier in Chapter 2 (determination of detector solid angle). In the case of dust particles of Figure 4, it has been shown that the Be yield in the region covering the peak structure around channel 520 is similar to the yield corresponding to Be foil. Therefore, the iteration process started by fitting the NRA spectrum and assuming only the presence of Be and D. Multiplication factor of the number of ^{3}He ions collected during measurement and the detector solid angle determined in such a way was used to assess the charge input needed to calculate first iterative concentrations of heavier elements present in the PIXE spectra (with B as invisible element in the iterative matrix procedure). The result was then used as another input for NRA analysis and after several iterations consistent result could be obtained.

As explained in Chapter 2, during the fit of NRA spectra it is very important to take into account geometrical correction due to large PDSSB detector solid angle. This is demonstrated in Figure 6, where the influence of geometrical effects on the analysis of NRA spectrum from the Figure 5 is clear on deuterium peak. While at 135 deg deuterium fit shows two peaks characteristic for 125 deg, our experimental spectrum has quite different shape, which can be well explained by taking in account geometrical effects due to the large detector solid angle. At the end of the iteration process we obtained the concentrations given in Table 1.

Table 1.Elemental concentrations for Figure 5.[1]

	Be	D	Ni	Cr	Fe	W	Cu	Ti
at%	91	3.3	2.9	0.8	0.6	0.9	0.5	0.02
w%	65	0.5	13.3	3.1	2.5	13	2.6	0.06

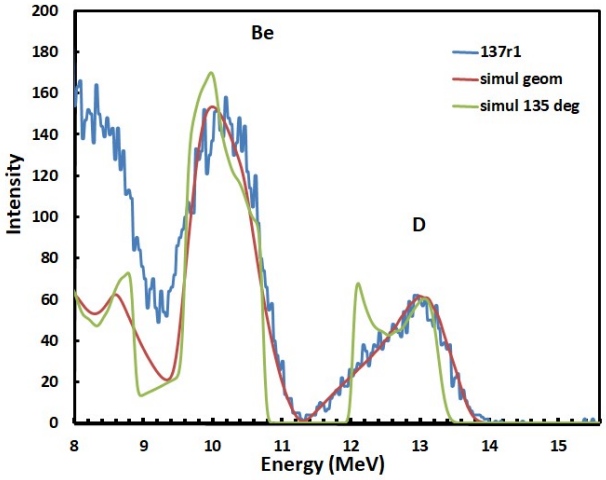

Figure 6 Influence of geometrical effects on the analysis of NRA spectra with the evident presence of deuterium. The same spectrum of the Figure 5 is shown.

Uncertainties of these results are combined from statistical and fit uncertainties and calibration uncertainties. In case of Ti combined uncertainty is estimated to 12%. For Ni, Cr, and Fe it is estimated to about 5%, and for W and Cu to about 7%. In case of Be and D this combined estimated uncertainty would be about 6%. However, uncertainties of NRA cross sections for ^{9}Be(^{3}He, po)^{11}B and ^{9}Be(^{3}He, αo)^{8}Be reactions should be added. In addition, we have to have in mind that this is semi-quantitative analysis, since we assumed that our dust particles are flat, thick and homogeneous, which is certainly only an approximation as shown in further SEM analysis, but justified with Be and D peak shape NRA simulations. The NRA simulation performed shows also that the thickness of Be is at least $1.4x10^{20}$ at/cm^2 or more, while D thickness is $2.2x10^{20}$ at/cm^2 or more.

Figure 7 shows dust particles located at the edge of the large conglomerate of particles on the left side (in reference to Figure 1). Associated spectra from the scanned area and from the region corresponding to the presence of W in the PIXE 2D map are shown at the Figure 8. Elemental composition of dust particles is very similar to the ones from the Figure 4, except that deuterium shows non-even distribution. Therefore, the total deuterium content in the region covered by dust particles is lower than in the previous case, as it can be clearly observed from the NRA spectrum (red line) at Figure 8.

The elemental concentrations obtained following the same iterative procedure are shown in Table 2. The PIXE spectra suggest that also some Mo could be present in the sample. The

[1]Average elemental concentrations obtained for the dust particles from the Figure 5, given as atomic percent (at %) and weight percent (w %). Uncertainties are discussed in the text.

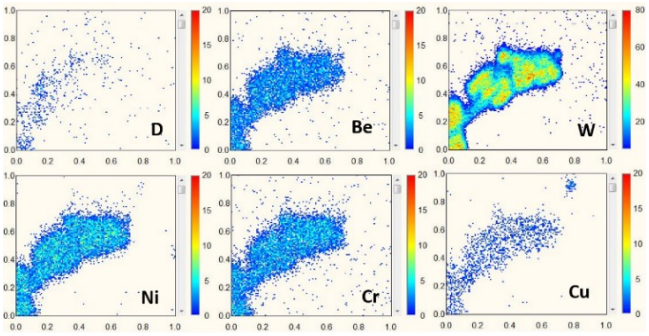

Figure 7 2D distribution maps of major elements from selected scanned area at the right edge of the region with high density of dust particles. Scan size is 320x320 μm^2 and resolution is 128x128 pixels.

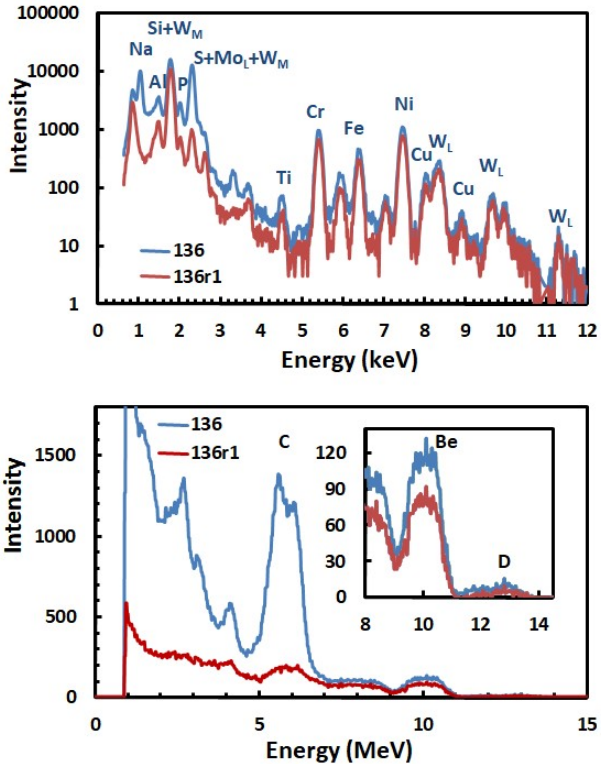

Figure 8 Respective PIXE and NRA spectra from the scanned area from Figure 7.

NRA simulation shows that the thickness of Be is at least $1.6x10^{20}$ at/cm^2 or more, while D thickness is $2.2x10^{20}$ at/cm^2 or more.

Table 2. Elemental concentrations for Figure 8.[2]

	Be	D	Ni	Cr	Fe	W	Cu	Ti
at%	96.7	0.5	1.2	0.4	0.3	0.5	0.2	0.01
w%	81	0.09	7.0	1.9	1.4	7.7	1.3	0.06

[2]Average elemental concentrations obtained for the dust particles from the Figure 8, given as atomic percent (at %) and weight percent (w %). Uncertainties are discussed in the text.

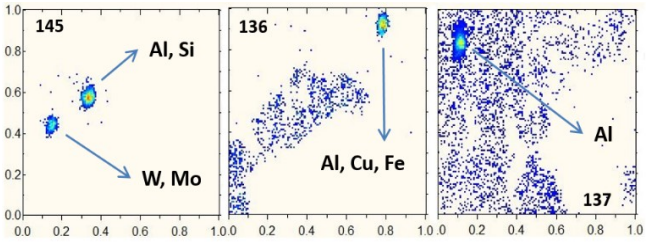

Figure 9 Small particles. In PIXE spectra one clearly shows only Al, two Al with Si or Cu and Fe. One is quite different with large concentrations of W and Mo (with relative mass concentrations W:Mo of about 2:1). NRA spectra show only carbon.

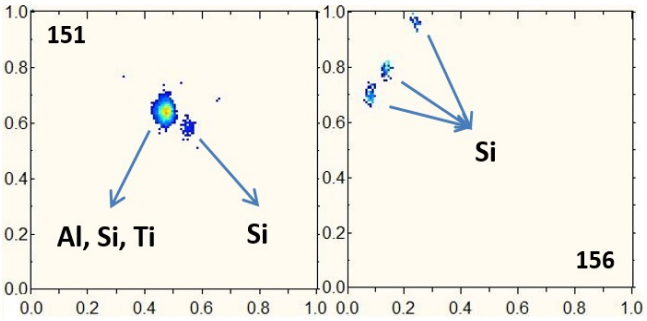

Figure 10 Another small particles with large Si content as seen by PIXE. Four in PIXE clearly show only Al, and one in addition some Al and Ti. NRA spectra show only carbon.

Uncertainties are similar as in the previous example, except for D where it is larger. It is clear from the Figure 8 that deuterium is not evenly distributed in all particles and that some of them have larger D concentrations then the others.

By moving along the marked area at Figure 1 towards the centre of the sticky pad, the density of dust particles drops considerably. A number of small particles, few of which were observed in the region on the left, increased a bit. Examples of such small particles are shown at Figures 9 and 10. Small particles containing Al and/or Si, in some cases accompanied with some other elements like Fe, Cu or Ti, were observed. One quite different particle was identified, containing W and Mo in concentration ratio of about 2:1.

Among such small particles, we have also observed several larger particles or conglomerates of particles far from the high

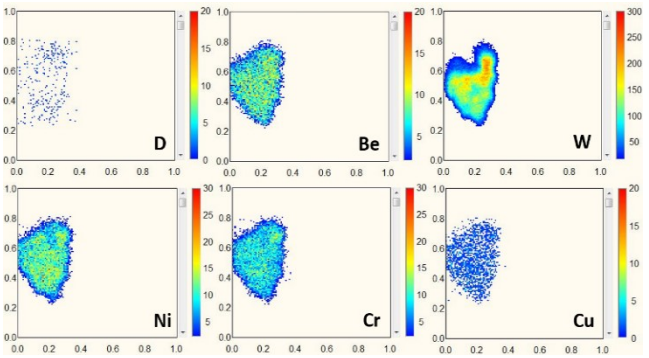

Figure 11 2D distribution maps of major elements from selected scanned area showing one isolated particle with the size of about 100 μm. Scan size is 320x320 μm^2 and resolution is 128x128 pixels.

Table 3. Elemental concentrations obtained for the black rectangle in Figure 12.[3]

	Be	D	Ni	Cr	Fe	W	Cu	Ti
at %	97.1	0.5	1.3	0.5	0.3	0.24	0.2	0.01
w %	83.7	0.09	7.1	2.2	1.4	4.3	1.1	0.06

density area on the left.

An example of one such particle is shown at Figure 11. As seen from PIXE and NRA spectra its constitution is very similar to the ones already discussed. The particle contains mainly Be, with some presence of W, Ni, Cr, Fe, Cu, Ti and unevenly distributed deuterium. Figure 11 shows two sets of PIXE/NRA spectra related to two selected areas marked at the 2D Be map at the Figure 11 as red and black rectangles. At higher energy part above the D peak, NRA shows possible traces of nitrogen.

Elemental concentrations related to the area marked with black rectangle were obtain following the same iterative procedureand shown at the Table 3. Obtained concentrations and level of uncertainties are similar to the ones related to those of other particle conglomerates.

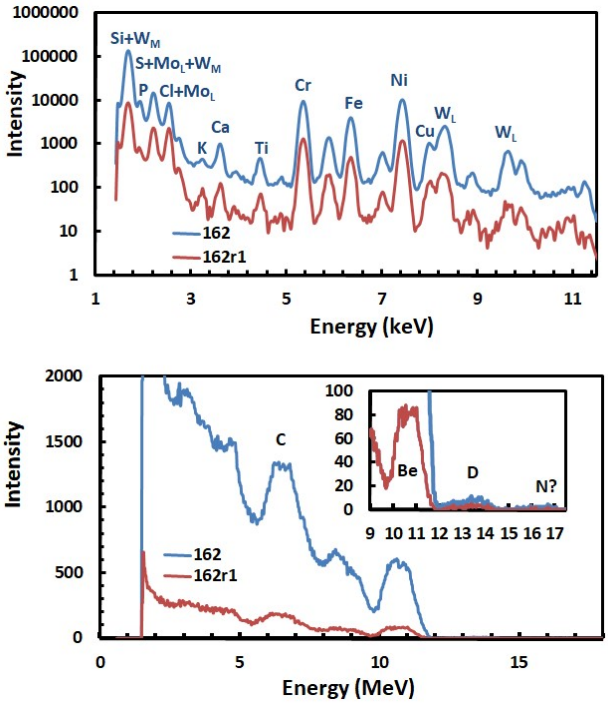

Figure 12 Respective PIXE and NRA spectra from the scanned area from Figure 11.

[3]Elemental concentrations obtained for the area marked with black rectangle at Be 2D map of the dust particle from the Fig. 12, given as atomic percent (at %) and weight percent (w %). Uncertainties are discussed in the text

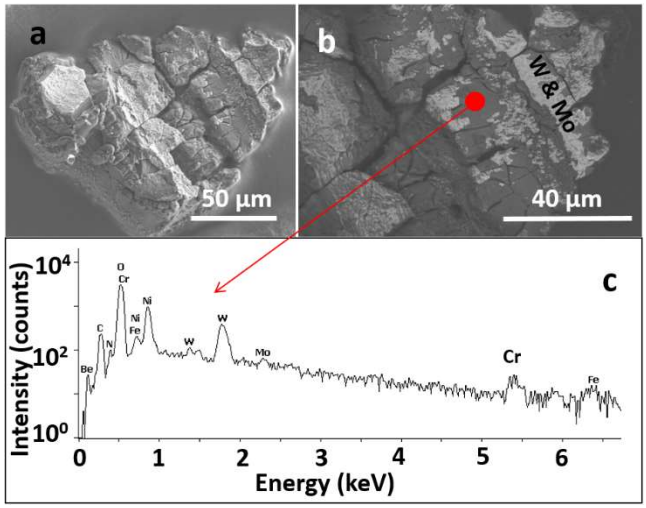

Figure 13 Microscopy images and X-ray spectrum of the dust particle: (a) secondary electron and (b) back-scattered electron images; (c) X-ray spectrum recorded in the position marked with a dot in image (b).

Figures 13 and 14 show complementary information obtained from this particle surface by SEM analysis. Figures 13 (a) and (b) show respectively secondary and back-scattered electron images of this dust particle. Figure 14 shows Secondary electron images of the same dust particle in different magnifications. The back-scattered electron image indicates surface areas of different atomic number (Z contrast). Darker parts are rich in low-Z elements, especially Be, while the main constituents of brighter areas are tungsten and molybdenum. The latter were most probably detached from the W-Mo coatings on the carbon-fibre composite tiles. This object is typical for the deposition zone on Tile 0, where layers reach thickness of 20-40 µm. The particle is fairly large, 100x120 µm, but one perceives quite fractured structure thus suggesting that the co-deposit may disintegrate to much smaller pieces. The SEM-EDS X-ray spectrum at Figure 13 (c) shows the existence of a mix of low-Z and high-Z elements: beryllium, carbon, nitrogen, nickel, chromium, iron, molybdenum and tungsten. The presence of these elements as detected by SEM-EDX from the sample surface (up to the depth of 1 µm) is in agreement with the PIXE, which however shows several additional elements and gives information from the surface and below to much larger depth. Figure 13 shows small Mo L peak at about 2.3 keV. Figure 12 shows related PIXE spectrum where the peak at the same position is observed and there it is marked as S+MoL+WM since it can be overlap of S Ka, Mo-La and with small contribution of W-M X-ray lines. Figure 3 shows that sticky pad contains S and therefore we performed quantitiative analysis in GupixWin without Mo (i.e. assuming that main contribution to this line is from parasitic S from the sticky pad and some contribution of W M line. The inclusion of Mo-L line in the GupixWin analysis results with possible concentration of Mo in the sample of about 0.8 w% or below. The PIXE spectra shown at Figures 5 and 8 are similar, and inclusion of Mo-L contribution in the analysis results with possible Mo concentrations of up to 2.9 w% and 1.1 w% respectively.

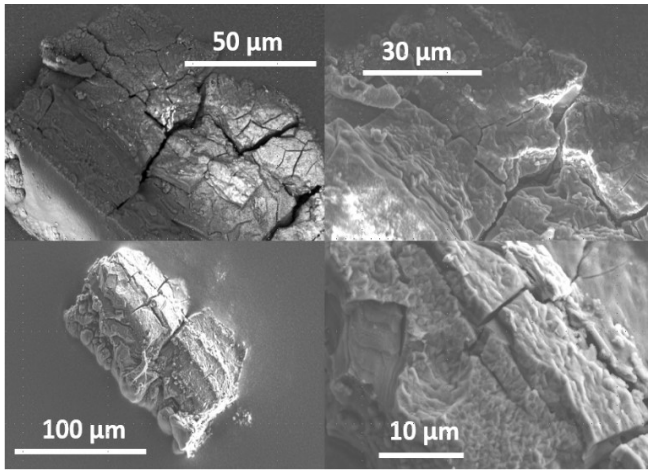

Figure 14 Secondary electron images of the same dust particle in different magnifications.

CONCLUSIONS

Simultaneous use of NRA and PIXE spectroscopies with 2D scanning of focused 3He ion beams over the areas of up to 1x1 mm^2 can be used for semiquantitative analysis of dust particles from tokamaks with metal like walls. Almost all major and minor elements can be detected, including deuterium. Due to low 3He ion currents it is necessary to use large area NRA detectors with large solid angle, which requires spectra integration over all the angles to obtain proper simulation of NRA spectra. Semiquantitative analysis can be obtained by iterative PIXE-NRA calculation procedure using GUPIX and SIMNRA analytical tools after calibration of the experimental setup with appropriate standards.

The method developed has been used for the analysis of dust particles sampled using a sticky carbon pad from the inner divertor tile after the second ILW campaign (2013-2014) comprising 19.5 h of plasma operation (13.5 h of X-point plasma) with total energy input of 201 GJ.

Two types of dust particles have been found:

1) NRA shows Be, with some D; in coincidence with Cr, Fe, Ni, Cu, W, seen by PIXE. Particles are present as thick 'layers', i.e. with Be not only on surface but spread to at least 10 to 15 µm. Beryllium concentrations are high, i.e. larger than 90 at%. Deuterium concentration is up to about 3.2 at% or lower. Among heavier elements, tungsten and nickel are major elements, accompanied with Cr and Fe, together with traces of Ti and Cu. These are particles from JET ILW D-T operation. These are particles of mixed columnar and stratified structure, detached from the deposition zone, shaped as thick Be-based layers, with presence of D, i.e. fusion fuel; and including W, Ni, Cr, Fe, Ti and Cu, showing origin of these particles, i.e. Be covered tiles. The results have shown non-uniform distribution of species in loosely bound deposits/dust particulates.

2) Smaller particles for which NRA shows only C (background carbon sticky tape pad) in coincidence with Na, Si S, P, K (background carbon sticky tape pad) and rich in Al and/or Si, in some cases accompanied with some other elements like Fe, Cu or Ti; with the exception of one quite different particle containing W and Mo in concentration ratio of about 2:1.

Most of those particles could most probably be contamination, i.e. not particles resulting from JET ILW D-T operation.

ACKNOWLEDGMENT

This work has been carried out within the framework of the EUROfusion Consortium and has received funding from the Euroatom research and training programme 2014-2018 under grant agreement No 633053. The views and opinions expressed herein do not necessarily reflect those of the European Commission.

REFERENCES

(1) Matthews, G. F.; Edwards, P.; Hirai, T.; Kear, M.; Lioure, A.; Lomas, P.; Loving, A.; Lungu, C.; Maier, H.; Mertens, P.; Neilson, D.; Neu, R.; Pamela, J.; Philipps, V.; Piazza, G.; Riccardo, V.; Rubel, M.; Ruset, C.; Villedieu, E.; Way, M.; the ITER-like Wall Project Team. *Phys. Scr*. **2007**, *2007*, 137-143.

(2) Matthews, G. F.; Beurskens, M.; Brezinsek, S.; Groth, M.; Joffrin, E.; Loving, A.; Kear, M.; Mayoral, M. L.; Neu, R.; Prior, P.; Riccardo, V.; Rimini, F.; Rubel, M.; Sips, G.; Villedieu, E.; de Vries, P.; Watkins, M. L.; EFDA-JET contributors. *Phys. Scr*. **2011**, *2011*, 014001-014001.

(3) Braams, B. J. Characterisation of Size, Composition and Origins of Dust in Fusion Devices, IAEA, 2013, https://www-nds.iaea.org/publications/indc/indc-nds-0607.pdf

(4) Merola, M.; Escourbiac, F.; Raffray, R.; Chappuis, P.; Hirai, T.; Martin, A. *Fusion Eng. Des.* **2014**, *89*, 890-895.

(5) Widdowson, A.; Alves, E.; Ayres, C. F.; Baron-Wiechec, A.; Brezinsek, S.; Catarino, N.; Coad, J. P.; Heinola, K.; Likonen, J.; Matthews, G. F.; Mayer, M.; Rubel, M.; JET-EFDA Contributors. *Phys. Scr.* **2014**, *2014*, 014010-014010.

(6) Fortuna-Zaleśna, E.; Grzonka, J.;Rubel, M.; Garcia – Carrasco, A.; Widdowson, A.; Baron – Wiechec, A.; Ciupiński, L.; JET Contributors. *Nucl. Mater. Energy* **2017**, *12*, 582-587.

(7) Fortuna-Zaleśna, E.; Grzonka, J.; Moon, S.; Rubel, M.; Petersson, P.; Widdowson, A.; JET Contributors. *Phys. Scr.* **2017**, *2017*, 014038-014038.

(8) Balden, M.; Endstrasser, N.; Humrickhouse, P. W.; Rohde, V.; Rasinski, M.; von Toussaint, U.; Elgeti, S.; Neu, R.; the ASDEX Upgrade Team. *Nucl. Fusion* **2014**, *54*, 073010-073010.

(9) Petersson, P.; Rubel, M.; Possnert, G.; Pegourie, B. *Phys. Scr.* **2011**, *2011*, 014014-014014.

(10) Petersson, P.; Rubel, M.; Possnert, G.; Brezinsek, S.; Pegouried, B. *Nucl. Instrum. Methods Phys. Res., Sect. B* **2012**, *B273*, 113-117.

(11) Bergsåker, H.; Petersson, P.; Bykov, I.; Possnert, G.; Likonen, J.; Koivuranta, S.; Coad, J. P.; Widdowson, A. M.; JET EFDA contributors. *J. Nucl. Mater.* **2013**, *438*, S668-S672.

(12) Bykov, I.; Bergsåker, H.; Petersson, P.; Likonen, J.; Possnert, G. *Nucl. Instrum. Methods Phys. Res., Sect. B* **2014**, *B332*, 280-285.

(13) Rubel, M.; Petersson, P.; Zhou, Y.; Coad, J. P.; Lungu, C.; Jepu, I.; Porosnicu, C.; Matveev, D.; Kirschner, A.; Brezinsek, S.; Widdowson, A.; Alves, E.; JET Contributors. *Nucl. Fusion* **2017**, *57*, 066027-066027.

(14) Coad, J. P.; Alves, E.; Barradas, N. P.; Baron - Wiechec, A.; Catarino, N.; Heinola, K.; Likonen, J.; Mayer, M.; Matthews, G. F.; Petersson, P.; Widdowson, A.; JET-EFDA Contributors. *Phys. Scr.* **2014**, *2014*, 014012-014012.

(15) Lagoyannis, A.; Tsavalas, P.; Mergia, K.; Provatas, G.; Triantou, K.; Tsompopoulou, E.; Rubel, M.; Petersson, P.; Widdowson, A.; Harissopulos, S.; Mertzimekis, T. J.; the JET contributors. *Nucl. Fusion* **2017**, *57*, 076027-076027.

(16) Baron - Wiechec, A.; Widdowson, A.; Alves, E.; Ayres, C. F.; Barradas, N. P.; Brezinsek, S.; Coad, J. P.; Catarino, N.; Heinola, K.; Likonen, J.; Matthews, G. F.; Mayer, M.; Petersson, P.; Rubel, M.; van Renterghem, W.; Uytdenhouwen, I.; JET-EFDA contributors. *J. Nucl. Mater.* **2015**, *463*, 157-161.

(17) Mayer, M.; Gauthier, E.; Sugiyama, K.; von Toussaint, U. *Nucl. Instrum. Methods Phys. Res., Sect. B* **2009**, *B267*, 506-512.

(18) Rubel, M.; Coad, J. P.; Likonen, J.; Philipps, V.; JET-EFDA Contributors. *Nucl. Instrum. Methods Phys. Res., Sect. B* **2009**, *B267*, 711-717.

(19) Jakšić, M.; Bogdanović Radović, I.; Bogovac, M.; Desnica, V.; Fazinić, S.; Karlušić, M.; Medunić, Z.; Muto, H.; Pastuović, Ž.; Siketić, Z.; Skukan, N.; Tadić, T. *Nucl. Instrum. Methods Phys. Res., Sect. B* **2007**, *B260*, 114-118.

(20) Bogovac, M.; Bogdanović, I.; Fazinić, S.; Jakšić, M.; Kukec, L.; Wilhelm, W. *Nucl. Instrum. Methods Phys. Res., Sect. B* **1994**, *B89*, 219-222.

(21) Mayer, M. SIMNRA User's Guide, Report IPP 9/113, Max-Planck-Institut für Plasmaphysik, Garching, Germany, 1997.

(22) Rauhala, E.; Barradas, N. P.; Fazinić, S.; Mayer, M.; Szilágyi, E.; Thompson, M. *Nucl. Instrum. Methods Phys. Res., Sect. B* **2006**, *B244*, 436-456.

(23) Campbell, J. L.; Boyd, N. I.; Grassi, N.; Bonnick, P.; Maxwell, J. A. *Nucl. Instrum. Methods Phys. Res., Sect. B* **2010**, *B268*, 3356-3363.

(24) Blaauw, M.; Campbell, J. L.; Fazinić, S.; Jakšić, M.; Orlic, I.; Van Espen, P. *Nucl. Instrum. Methods Phys. Res., Sect. B* **2002**, *B189*, 113-122.

(25) https://www-nds.iaea.org/exfor/ibandl.htm

(26) Alimov, V. Kh.; Mayer, M.; Roth, J. *Nucl. Instrum. Methods Phys. Res., Sect. B*, **2005**, *B234*, 169-175.

(27) Barradas, N. P. *Nucl. Instrum. Methods Phys. Res., Sect. B* **2015**, *B346*, 21-25.

(28) Wolicki, E. A.; Holmgren, H. D.; Johnston, R. L.; Geer Illsley, E. *Phys. Rev.* **1959**, *116*, 1585.

(29) Bilwes, B.; Bilwes, R.; Ferrero, J. L.; Garcia, A. *J. Phys. (Paris).* **1978**, *39*, 805-814.

(30) Lin, B. S.; Hou, W. S.; Wen, M. *Chin. J. Phys. (Taipei, Taiwan)*. **1981**, *19*, 99-105.

(31) McIntyre Jr., L. C.; Leavitt, J. A.; Ashbaugh, M. D.; Borgardt, J.; Andrade, E.; Rickards, J.; Oliver, A. *Nucl. Instrum. Methods Phys. Res., Sect. B* **1996**, *B118*, 219-223.

(32) Terwagne, G.; Cohen, D. D.; Collins, G. A. *Nucl. Instrum. Methods Phys. Res., Sect. B* **1994**, *B84*, 415-420.

(33) Kuan, H. M.; Bonner, T. W.; Risser, J. R. *Nucl. Phys.* **1964**, *51*, 481-517.

(34) Tong, S. Y.; Lennard,W. N.; Alkemade, P. F. A.; Mitchell, I. V. *Nucl. Instrum. Methods Phys. Res., Sect. B* **1990**, *B45*, 91-94.

(35) Geer Illsley, A.; Holmgren, H. D.; Johnston, R. L.; Wolicki, E. A. *Phys. Rev.***1957**, *107*, 538-539.

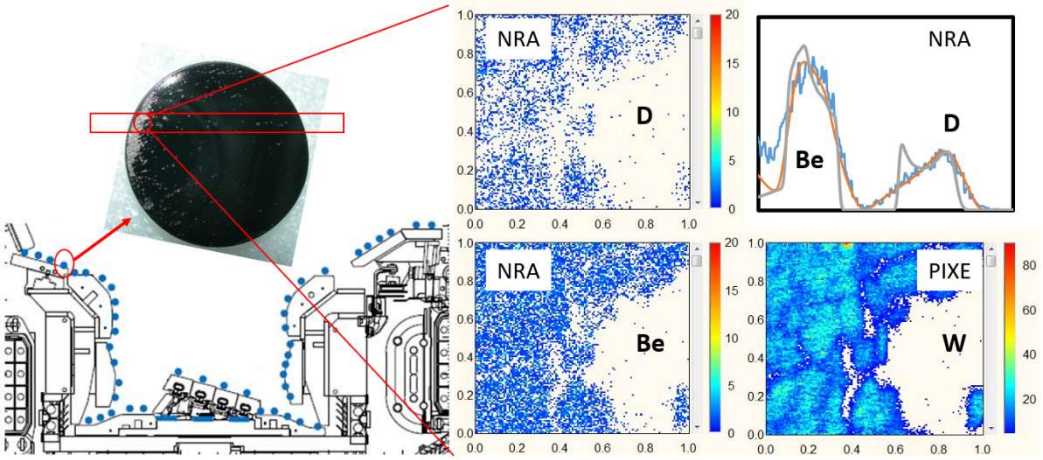

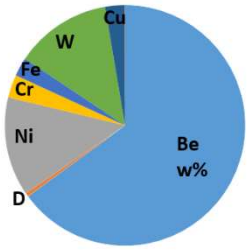

Be > 90 at%
D < 3.5 at%

For Table of Contents only